This article has been accepted for publication in IEEE Transactions on Industry Applications. This is the author's version which has not been fully edited and content may change prior to final publication. Citation information: DOI 10.1109/TIA.2022.3213002

Direct Model Predictive Control of Synchronous Reluctance Motor Drives

Jacopo Riccio, *Student Member, IEEE*, Petros Karamanakos, *Senior Member, IEEE*, Shafiq Odhano, *Member, IEEE*, Mi Tang, *Member, IEEE*, Mauro Di Nardo, *Member, IEEE*, and Pericle Zanchetta, *Fellow, IEEE*

***Abstract*—This paper investigates a finite-control set model-predictive control (FCS-MPC) algorithm to enhance the performance of a synchronous reluctance machine drive. Particular emphasis is placed on the definition of the cost function enabling a computationally light implementation while targeting good transient and steady-state performance. In particular, this work proposes the inclusion of an integral term into the cost function to ensure zero steady-state errors thus compensating for any model inaccuracies. A control effort term is also considered in the formulation of the cost function to achieve a high ratio between the sampling frequency and the average switching frequency. After a comprehensive simulation study showing the advantages of the proposed approach over the conventional FCS-MPC for a wide range of operating conditions, several experimental test results are reported. The effectiveness of the proposed control approach, including a detailed analysis of the effect of the load and speed variations, is thus fully verified providing useful guidelines for the design of a direct model predictive controller of synchronous reluctance motor drives.**

***Index Terms*—Synchronous reluctance machine, finite control set model predictive control, two-level voltage-source inverter, steady-state performance.**

I. Introduction

In many industrial applications, synchronous reluctance (SyRel) motor drives are gaining significant attention as viable alternative to conventional drives based on induction and permanent magnet synchronous motors (PMSMs) thanks to their satisfactory performance at a competitive cost [1]. The lack of winding and rare-earth-based permanent magnets on the rotor makes this machine topology less susceptible to raw material price fluctuations, guaranteeing a stable supply chain. On the other hand, the disadvantages of SyRel motors include the low power factor, high torque ripple, and remarkably non-linear magnetic behavior, which inevitably complicate the control algorithm [2], [3]. The first two disadvantages are usually mitigated during the machine design aimed at maximizing the machine anisotropy and minimization of the torque oscillation [4].

Jacopo Riccio, Mi Tang, Mauro Di Nardo, and Pericle Zanchetta are with the Department of Electrical and Electronic Engineering, University of Nottingham, Nottingham, UK; e-mail:Jacopo.Riccio1@nottingham.ac.uk, mi.tang@nottingham.ac.uk, mauro.dinardo4@nottingham.ac.uk pericle.zanchetta@nottingham.ac.uk

Petros Karamanakos is with the Faculty of Information Technology and Communication Sciences, Tampere University, 33101 Tampere, Finland; e-mail: p.karamanakos@ieee.org

Shafiq Odhano is with the School of Engineering, Newcastle University, Newcastle Upon Tyne, UK; e-mail: shafiq.odhano@newcastle.ac.uk

Regarding the non-linear magnetic behavior, this is tackled with the adoption of ad-hoc control strategies with the target of achieving the desired performance independently from the operating point. The most commonly used control approach is field-oriented control (FOC) based on proportional-integral (PI) controllers [5]. Although its implementation is relatively straightforward, such a control method is not the most suitable for non-linear systems like SyRel motor drives. Indeed, its performance varies substantially depending on the operating point, and if a thorough offline tuning procedure is not followed (i.e., gain scheduling) inferior performance may result, and even stability issues may appear. Direct torque control (DTC) is another possible solution for SyRel machine drives [6]. This method is characterized by its simplicity and wide applicability, even though it is prone to high current ripples.

An alternative to the above-mentioned control techniques is model predictive control (MPC), especially in its direct control version, known as finite-control set MPC (FCS-MPC) [7]. Complex and constrained non-linear systems, such as SyRel motor drives, can benefit from this control approach, especially when an increased granularity of switching is achievable [8], [9], i.e., a high ratio between the sampling frequency and the average switching frequency.

In order to implement MPC strategies, two stringent hardware criteria must be satisfied. Firstly, the computing capability of the controller must be sufficiently high to execute the control algorithm in real time. This is addressed by economically affordable digital control chips based on field-programmable gate arrays (FPGAs) and digital signal processors (DSPs) capable of handling computationally demanding algorithms like FCS-MPC. Furthermore, the power modules of the driving converter must ensure high switching frequencies while respecting the physical limitations imposed by the semiconductor devices. The adoption of silicon-carbide (SiC) power switches allows keeping the operating temperature within the safe working region of the devices while running at very high switching frequencies [10], [11].

According to the working principle of FCS-MPC, the system behavior is predicted for all feasible actuating commands. The one that minimizes a given cost function is selected and applied to the power converter. Typically, the cost function definition merely considers the error of the tracking terms as in [12]. Nevertheless, [8] states that the lack of the control effort penalization leads to a low granularity of switching and, consequently, a poor performance. Several studies considered

This article has been accepted for publication in IEEE Transactions on Industry Applications. This is the author's version which has not been fully edited and content may change prior to final publication. Citation information: DOI 10.1109/TIA.2022.3213002

the control effort in their cost functions, such as in [13], where the penalization in the change of the switching state results in a reduction in the commutation losses of a matrix converter. The same practice was adopted in [14] and [15] to control a PMSM and a SyRel motor, respectively. The latter provides simulation results focused on extending the prediction horizon to enhance the MPC performance at steady state.

Another common difficulty with FCS-MPC is that inaccurate knowledge of the system model can negatively influence the reference tracking performance of the controller [16]. When it comes to SyRel motor drives, a precise identification procedure of the nonlinear magnetic model is required, unless the controller inherently compensates for any potential model mismatches. A few approaches have been proposed, mainly applied to PMSMs, to imporve the robustness of FCS-MPC. In [17], [18], the integral of the state was included in the cost function, resulting in an augmented prediction model of the PMSM. In [19], a real-time least-squares system identification was adopted to correct any set-point deviations. In [20], an integral term was added to the cost function without augmenting the system state. However, it has to be underlined that including an integral term within the cost function, calculated based on the state prediction, increases the algorithm complexity and its computational burden.

This work, based on [9], investigates an FCS-MPC method for SyRel motor drives with particular emphasis on the formulation of the cost function. Specifically, the typical cost function of FCS-MPC that solely accounts for the stator current reference tracking is augmented by introducing two terms, namely a term to integrate the tracking error and a control effort term. The former term enhances the steady-state performance of the drive as it increases the controller robustness to parameter variations, model mismatches, etc. The second term allows for direct control of the switching frequency, thus it enables an increase of the switching granularity and, consequently, an improved steady-state performance in terms of stator current distortions.

To demonstrate the effectiveness of the proposed control strategy, an extensive simulation and experimental study are performed. As shown, compared with conventional FCS-MPC, the proposed method exhibits superior steady-state performance over a wide range of operating points, such as different loads and speeds, while achieving a high degree of robustness. Moreover, the favorable dynamic behavior that typically characterizes FCS-MPC is still present. This advantageous performance is achieved with only a small computational overhead due to the additional cost function terms. Regardless of this, the presented control technique, being an optimal control method that relies on the real-time solution of an optimization problem, still requires more computational resources than conventional control solutions, such as linear control techniques. Hence, it is not well-suited for low-cost microprocessors. Nevertheless, given the fall in the cost of powerful microprocessors and the increase in their computational power, the potential of the proposed control scheme can be fully harvested in the near future.

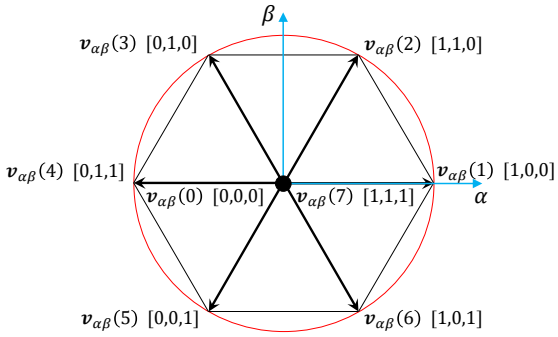

Fig. 1: Voltage vectors and corresponding switching positions.

This paper is organized as follows. The two-level voltage-source inverter (2L-VSI) and the SyRel motor prediction models are described in Section II. The FCS-MPC algorithm derivation is given in Section III. Simulation results are presented in Section IV to verify the superior performance of the proposed control approach when compared with the conventional one for various operating points. Section V reports the experimental findings in several operating scenarios. Lastly, the overall achievements are summarized in Section VI.

II. Synchronous Reluctance Machine Drive Prediction Model

The 2L-VSI and SyRel motor mathematical models used for the implementation of the proposed control technique are discussed in this section.

A. 2L-VSI Model

In a stationary orthogonal reference frame ($\alpha\beta$) the eight switch positions ($n = 0, 1..., 7$) of the 2L-VSI form a hexagon as shown in Fig. 1. The following are the three-phase voltage components:

$$\begin{cases} v_a(n) = \frac{V_{dc}}{3}\left[2S_a(n) - S_b(n) - S_c(n)\right] \\ v_b(n) = \frac{V_{dc}}{3}\left[2S_b(n) - S_a(n) - S_c(n)\right] \\ v_c(n) = \frac{V_{dc}}{3}\left[2S_c(n) - S_a(n) - S_b(n)\right] \end{cases} \tag{1}$$

where V_{dc} is the dc-link voltage set by the power supply, $S_a(n)$, $S_b(n)$, and $S_c(n)$ are the configurations of the corresponding inverter legs, yielding eight switching positions as reported in Table I. As shown in Fig. 1, these configurations result in six active voltage vectors $\boldsymbol{v}_{\alpha\beta}(1, 2, \ldots, 6)$, and two zero voltage vectors $\boldsymbol{v}_{\alpha\beta}(0)$, $\boldsymbol{v}_{\alpha\beta}(7)$.

The dq-voltage vectors can be obtained by using the following transformation:

$$\boldsymbol{v}_{dq}(n) = \boldsymbol{P} \cdot \boldsymbol{v}_{abc}(n) \tag{2}$$

where $\boldsymbol{v}_{abc}(n)$ is the three-phase voltage vector. The Clarke and Park transformations are merged, forming the rotation matrix $\boldsymbol{P}$, which is a function of the electrical angle θ_r.

This article has been accepted for publication in IEEE Transactions on Industry Applications. This is the author's version which has not been fully edited and content may change prior to final publication. Citation information: DOI 10.1109/TIA.2022.3213002

TABLE I: 2L-VSI switching positions.

n	0	1	2	3	4	5	6	7
$S_a(n)$	0	1	1	0	0	0	1	1
$S_b(n)$	0	0	1	1	1	0	0	1
$S_c(n)$	0	0	0	0	1	1	1	1

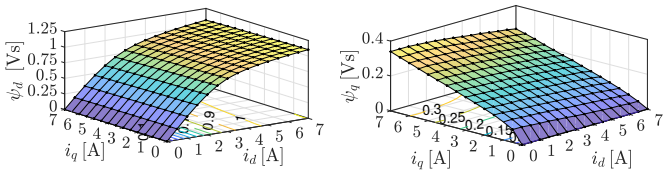

(a) (b)

Fig. 2: Magnetic model identified experimentally. (a) d-flux linkage versus d-and q-current. (b) q-flux linkage versus d- and q-current

.

B. SyRel Motor Non-linear Model

FCS-MPC bases its working principle on predicting the system state. Hence, having an accurate representation of the plant is critical. The system is modeled in a synchronous reference frame (dq coordinates) rotating at the electrical speed ω_r which relates to the mechanical speed via the number of pole pairs p. In this reference frame, the electrical variables are represented by constant vectors. The discrete-time domain drive model is deduced as follows by using the forward Euler discretization:

$$\boldsymbol{i}_{dq}^{\,k+1}(n) = \boldsymbol{i}_{dq}^{\,k} + T_s \boldsymbol{L}^{-1}\left[\boldsymbol{v}_{dq}^{k}(n) - R_s \boldsymbol{i}_{dq}^{\,k} + \boldsymbol{Q}\omega_r \boldsymbol{\psi}_{dq}^{k}\right] \quad (3)$$

The superscript k on the right-hand side of (3) denotes the current time step, whereas $k+1$ on the left-hand side denotes the next time step, and T_s stands for the sampling interval between the two samples. The term $\boldsymbol{i}_{dq}^{\,k+1}(n)$ refers to the stator current prediction in dq coordinates, evaluated for each configurable switch position ($n = 0, 1, 2, \ldots, 7$) of the 2L-VSI. The matrix $\boldsymbol{Q} = \begin{bmatrix} 0 & -1 \\ 1 & 0 \end{bmatrix}$ performs a counter-clockwise rotation by 90^o. R_s is the stator resistance, while the actuating voltage vector $\boldsymbol{v}_{dq}^{k}(n)$ is defined in (2). The measured current vector is represented by $\boldsymbol{i}_{dq}^{\,k}$. The symbols $\boldsymbol{L^{-1}}$ and $\boldsymbol{\psi}_{dq}^{k}$ indicate the inverse of the differential inductance matrix and the magnetic flux vector, respectively, both varying with the current vector.

Due to the direct and cross-magnetization effects, both d- and q-axis flux linkages (ψ_d, ψ_q) show highly nonlinear behaviors with both the d- and q-axis currents components (i_d, i_q). The flux-versus-current characteristics are derived experimentally by performing offline tests according to the procedure described in [21], and the results are shown in Fig. 2. The resulting apparent inductances can be calculated as:

$$L_d(i_d, i_q) = \frac{\psi_d(i_d, i_q)}{i_d} \quad , \quad L_q(i_d, i_q) = \frac{\psi_q(i_d, i_q)}{i_q}. \quad (4)$$

The peculiarity of the SyRel machine lies in how the apparent inductance differs from the incremental inductance matrix

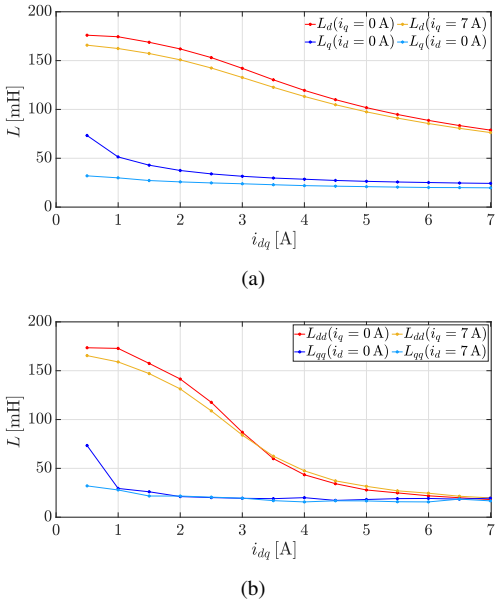

(a)

(b)

Fig. 3: (a) Apparent inductances L_d, L_q. (b) Incremental inductances L_{dd}, L_{qq}.

$\boldsymbol{L} = \begin{bmatrix} L_{dd} & L_{dq} \\ L_{qd} & L_{qq} \end{bmatrix}$, whose components can be numerically evaluated from the flux linkages and the current components as

$$L_{dd} = \frac{\partial \psi_d}{\partial i_d} \approx \frac{\psi_{d+1}^{q} - \psi_d^q}{\Delta i} \quad (5a)$$

$$L_{qq} = \frac{\partial \psi_q}{\partial i_q} \approx \frac{\psi_{q+1}^{d+1} - \psi_q^d}{\Delta i} \quad (5b)$$

$$L_{dq} = \frac{\partial \psi_d}{\partial i_q} \approx \frac{\psi_{d+1}^{q+1} - \psi_d^q}{\Delta i} \quad (5c)$$

$$L_{qd} = \frac{\partial \psi_q}{\partial i_d} \approx \frac{\psi_{q+1}^{d} - \psi_q^d}{\Delta i}. \quad (5d)$$

In (5), the term "Δi" is the fixed current step corresponding to two consecutive magnetic flux points. Subscripts identify the flux map, and superscripts denote to which orthogonal current a specific map is referred. The apparent inductance terms L_d and L_q are represented in Fig. 3(a). The terms L_{dd} and L_{qq} are the direct and quadrature incremental inductance components respectively, shown in Fig. 3(b). The quantities L_{dq} and L_{qd} are the cross magnetization inductance, resulting in non-zero terms. An accurate prediction model is required to guarantee high performance in model-based controllers, see, e.g., [22]. Any model mismatch can adversely deteriorate the accuracy of the predictions and, subsequently, the system behavior. Hence, self-axis non-linearities, and cross-saturation phenomena need to be fully known. To this end, the flux-current maps represented in Fig. 2 are stored in 2D look-up tables (LUTs) and used online for real-time control of the SyRel motor.

This article has been accepted for publication in IEEE Transactions on Industry Applications. This is the author's version which has not been fully edited and content may change prior to final publication. Citation information: DOI 10.1109/TIA.2022.3213002

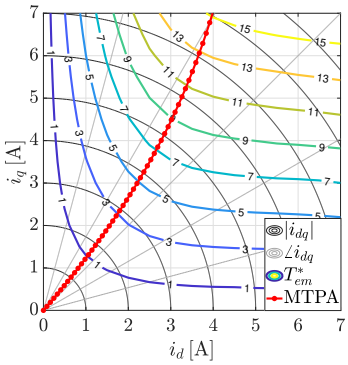

Fig. 4: Evaluated maximum torque per Ampere trajectory.

The electromagnetic torque T_{em} can be estimated knowing the flux versus current maps as:

$$T_{em} = \frac{3}{2} p \left(\boldsymbol{\psi}_{dq} \times \boldsymbol{i}_{dq} \right). \tag{6}$$

The maximum torque per ampere (MTPA) trajectory is evaluated offline [23] and stored as a 2D LUT, and it is represented in Fig.4.

III. Direct Model Predictive Control with Reference Tracking

Direct MPC, often referred to as FCS-MPC, is used to control the current of a SyRel motor drive. The major purpose of the controller is to accomplish precise current setpoint tracking while keeping the switching frequency reasonably low to reduce the switching losses. The accuracy of the prediction model (3) is critical to the effectiveness of the controller because FCS-MPC essentially behaves as a proportional controller. As a result, any existing model inconsistencies might amplify potential tracking problems.

A computationally expensive solution to this problem consists of implementing self-commissioning identification approaches and/or elaborated observers to the control strategy. In this work, a more computationally efficient approach is adopted to tackle this issue, i.e., by incorporating an integrating element into the cost function to compensate for any model inaccuracies and steady-state errors.

Given all the above, the cost function that can tackle all the aforementioned challenges can be defined as the sum of the (squared) 2-norm of the current errors plus an integrating term and a control effort term:

$$J(n) = \left\| \boldsymbol{i}^{k+1}_{dq,err}(n) + \boldsymbol{W}_{i_{dq}} T_s \left(\sum_{j=0}^{m} \boldsymbol{i}^{k-j}_{dq,err} \right) \right\|^2_2 + \lambda_u \left\| \Delta \boldsymbol{S}^k(n) \right\|^2_2 \tag{7}$$

where the error between the references i^{*k+1}_d, i^{*k+1}_q and the prediction components $i^{k+1}_d(n)$, $i^{k+1}_q(n)$ at the next time step $k+1$ defined in (3) is calculated as

$$\boldsymbol{i}^{k+1}_{dq,err}(n) = \boldsymbol{i}^{*k+1}_{dq} - \boldsymbol{i}^{k+1}_{dq}(n) \tag{8}$$

while the current error at step k, i.e., $i^k_{dq,err}$ is:

$$\boldsymbol{i}^{k}_{dq,err} = \boldsymbol{i}^{*k}_{dq} - \boldsymbol{i}^{k}_{dq} \tag{9}$$

The integrals of the current errors are evaluated at every sample j for ℓ times. The term $\boldsymbol{i}^{k-j}_{dq,err}$ is the previously calculated integral of the errors. $\boldsymbol{W}_{i_{dq}}$ is a diagonal matrix whose nonzero entries are two gains tuned in a trial-and-error fashion.

The first (squared) 2-norm in (7) includes two terms, i.e., the current errors and the integral of the error terms. By doing so, the integral of the error depends on the actuating commands (n) thanks to the cross-product. This term is calculated by considering the difference between the reference and the feedback current signals.

The control effort factor is defined as:

$$\Delta \boldsymbol{S}^k(n) = \boldsymbol{S}^k_{abc}(n) - \boldsymbol{S}^{k-1}_{abc} \tag{10}$$

where the term $\boldsymbol{S}^k_{abc}(n) = [S_a(n)\ S_b(n)\ S_c(n)]^T$ is evaluated for each configuration of the 2L-VSI ([0,0,0], [1,0,0], ... [1,1,1]), while $\boldsymbol{S}^{k-1}_{abc}$ represents the three-phase switch position applied at the previous time step $k-1$. The values that the control effort factor $\Delta \boldsymbol{S}^k(n)$ can assume are listed in Table II. The control effort term penalizes the change in the switch position, allowing the minimization of the average switching frequency. In other words, it enables a more beneficial granularity of the switching, defined as the ratio between the sampling frequency ($f_s = 1/T_s$) and the average switching frequency $\bar{f}_{sw}$, thus permitting operation in a quasi-continuous time domain with lower current distortions [8]. The weighting factor $\lambda_u > 0$ is used to create a high ratio and consequently fine switching granularity. The control effort penalization is not included in conventional FCS-MPCs, i.e., $\lambda_u = 0$. This implies that the switching frequency is not directly controlled, but merely limited by the sampling frequency, which defines a theoretical upper limit, i.e., $\bar{f}_{sw} = f_s/2$. As a consequence, conventional FCS-MPC achieves poor granularity of switching, which affects the drive performance, as indicated in the next section. Hence, the aim is to have as high a sampling frequency as possible and tune λ_u such that the average switching frequency is reduced, and, consequently, fine granularity of switching is achieved as experimentally verified in Section IV. Referring to Fig. 5, given the electrical angle and measured phase currents i_a, i_b, i_c, the prediction (3) can be evaluated for each vector n at the next sampling instant. The cost function is then evaluated to determine the optimum vector aiming to achieve the desired behavior, and to send the corresponding gate signals $\boldsymbol{S}_{abc}$ to the three legs of the 2L-VSI.

IV. Simulation Results

In this section, the performance of the proposed control strategy is evaluated by analyzing several simulations results

TABLE II: Control effort list of values for each configuration change.

n	**0**	**1**	**2**	**3**	**4**	**5**	**6**	**7**
0	0	1	2	1	2	1	2	3
1	1	0	1	2	3	2	1	2
2	2	1	0	1	2	3	2	1
3	1	2	1	0	1	2	3	2
4	2	3	2	1	0	1	2	1
5	1	2	3	2	1	0	1	2
6	2	1	2	3	2	1	0	1
7	3	2	1	2	1	2	1	0

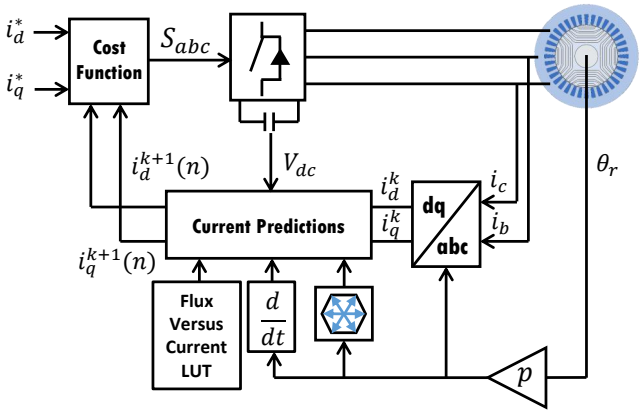

Fig. 5: Block diagram of FCS-MPC for a SyRel motor drive.

in terms of current total demand distortion (TDD_i) and average switching frequency ($\bar{f}_{sw}$), which are defined as:

$$\bar{f}_{sw} = \lim_{\ell\to\infty} \frac{1}{\nu \ell T_s} \sum_{z=0}^{\ell-1} ||\Delta \boldsymbol{S}_{abc}(z)||_1 \tag{11a}$$

$$\text{TDD}_i = \frac{\sqrt{\sum_{n\neq 1} i_n^2}}{I_n} \tag{11b}$$

In the definition of f_{sw}, ν is the number of power switches of the adopted converter, which is six for a 2L-VSI, and ℓ is the number of samples.

The estimation of the average switching frequency in real time is not an easy task due to finite storage constraints. In [24], the switching frequency is considered as a state variable and it is directly controlled. In this work, a low-pass filter (LPF) is adopted to online calculate the moving average switching frequency (11a). The mean value is post-processed and computed over an integer number of electrical periods. The TDD_i metric takes into account the energy spread over all harmonics except for the fundamental, and it gives finite results also when the fundamental harmonic is close to zero (as the denominator is the rated current, i.e., I_n). In a similar fashion to f_{sw}, TDD_i is calculated in a post-processing stage over an integer number of electrical periods, and averaged over the three phases.

A set of simulations of the proposed control approach, whose block diagram is reported in Fig. 5, has been performed

Variable	**Symbol**	**Value**	**Unit**
Stator Resistance	R_s	3.15	Ω
Rated Torque	T_{em}	14	Nm
Rated Speed	ω_m	1500	rpm
Rated Power	P_n	2.2	kW
Rated Current	I_n	5.5	A
Rated Voltage	V_n	400	V
Pole Pairs	p	2	#

TABLE III: SyRel motor nameplate.

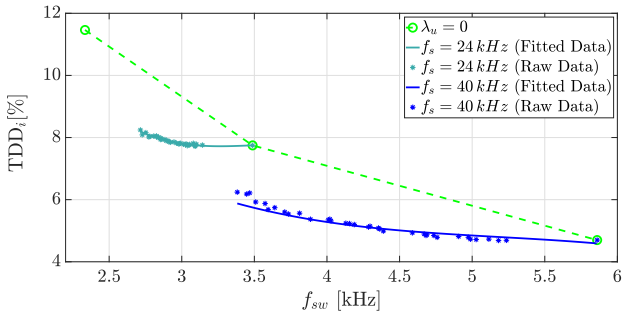

Fig. 6: Trade-off curves between current TDD_i and switching frequency at various λ_u and full-load ($i_d = i_q = 5.5\,\text{A}$; $\omega_m = 1500\,\text{rpm}$, $0 < \lambda_u < 0.056$).

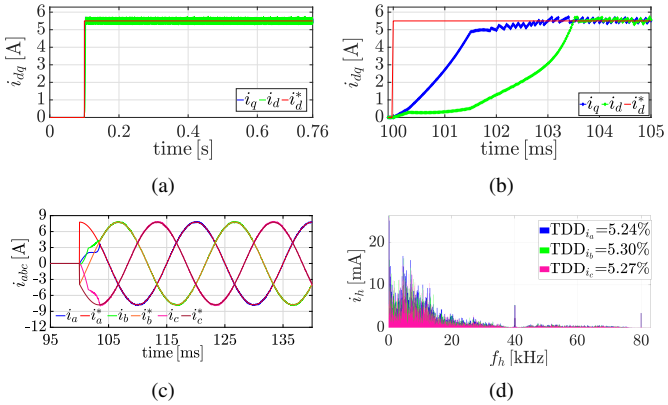

Fig. 7: (a) dq-current reference tracking ($f_s = 40\,\text{kHz}$, $\bar{f}_{sw} \approx 4020\,\text{Hz}$, and $\lambda_u = 0.0384$). (b) dq-current reference tracking transients. (c) a-, b-, and c-phase currents reference tracking. (d) a-, b-, and c-phase current harmonic spectra.

considering a SyRel motor with the nameplate data reported in Table III. The analysis has been carried out by keeping the current references, the rotational speed, and the dc-link voltage fixed and varying the sampling frequency and λ_u. In particular, the simulations have been carried out at full load, i.e., the current references were set to $5.5\,\text{A}$ on both d- and q-axis. The dc-link was set to $600\,\text{V}$, and the mechanical rotational speed to $1500\,\text{rpm}$. The current control tests are performed within a time window of $0.76\,\text{s}$, lasting long enough to have a periodicity over one mechanical turn. The model of the SyRel motor includes the identified magnetic model curves given in Figs. 2(a) and 2(b) implemented as a 2D LUT. The

This article has been accepted for publication in IEEE Transactions on Industry Applications. This is the author's version which has not been fully edited and content may change prior to final publication. Citation information: DOI 10.1109/TIA.2022.3213002

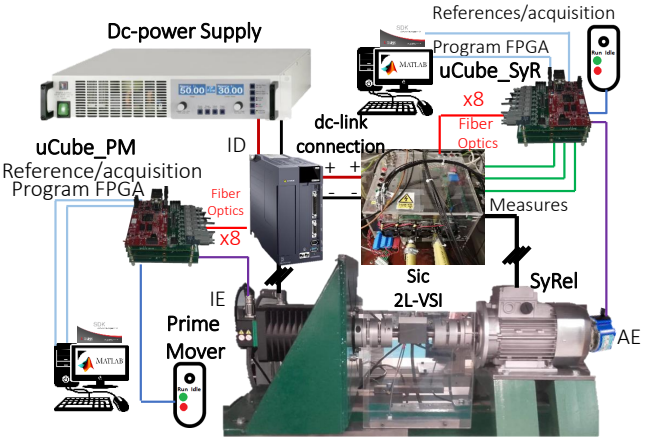

Fig. 8: Test bench configuration.

converter model is based on (1), and the dead-time effect is neglected. In Fig. 6, the resulting trade-off curves between the TDD_i and the average switching frequency ($\bar{f}_{sw}$) are shown. In particular, the conventional FCS-MPC (i.e., $\lambda_u = 0$), and the one proposed including the control effort term are represented for two sampling frequencies, i.e. $f_s = 24\,\text{kHz}$, $f_s = 40\,\text{kHz}$. The introduction of the control effort term (i.e., when $\lambda_u > 0$) allows achieving a lower current distortion over a wide range of switching frequencies and for different sampling frequencies compared to the performance obtained with $\lambda_u = 0$.

Considering the same switching frequency, i.e., $\bar{f}_{sw} \approx 4$ kHz, about 25% improvement of the current TDD_i is obtained. The benefit in terms of TDD_i over the conventional approach increases as λ_u increases for a given sampling frequency f_s. Higher sampling frequencies allow achieving a wider range of switching frequencies. Indeed, the blue line is wider than the dark green line, both calculated considering the same range of λ_u. A trial-and-error procedure was considered to tune λ_u to identify the trend shown. The dq-current reference tracking is shown in Figs. 7(a) and 7(b), whereas the measured a-, b-, and c-phase stator currents are shown in Fig. 7(c) for operation at $f_s = 24\,\text{kHz}$ and $\bar{f}_{sw} \approx 4$ kHz ($\lambda_u = 0.0384$). Fig. 7(d) reports the harmonic spectrum of the phase currents, confirming the low current TDD_i.

V. Experimental Results

The test rig layout (see Fig. 8) consists of the SyRel machine (whose details are reported in Table III) driven by a SiC 2L-VSI fed by a controllable dc-power supply. A prime mover (PM) driven by an industrial drive (ID) is mechanically coupled to the SyRel under test. The two converters share the same dc-link. The control algorithm was executed in real time on the control platform introduced in [25]. During the tests the average dc-link voltage was 300 V fixed by the dc-power supply and the industrial drive rated voltage. Each test lasted at least twenty electrical periods for accurate computations of the TDD_i. In the following, several experimental test campaigns are reported to assess the effectiveness of the proposed FCS-MPC to guarantee zero steady-state reference tracking errors and a reduced TDD_i compared with conventional FCS-MPC. When powerful microprocessors are used based on an FPGA or a system-on-chip solution, such as the one employed for this work [25], then a higher f_s can be used. This increases the granularity of switching and thus the system performance.

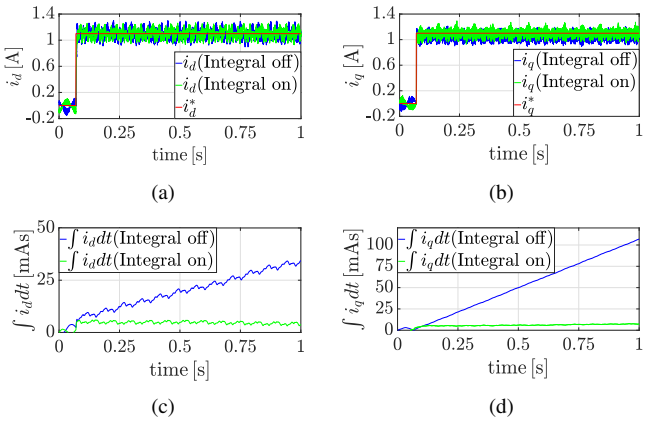

Fig. 9: Steady-state performance under 50% magnetic flux prediction error. (a) d-current tracking with and without integral (b) q-current tracking with and without integral. (c) Integral of the d-current error over time with and without integral. (d) Integral of the q-current error over time with and without integral.

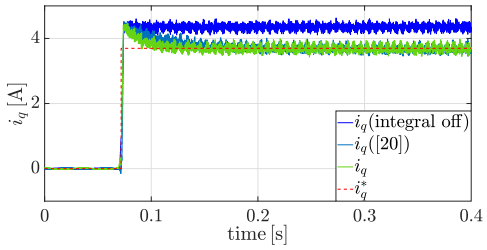

Fig. 10: Assessment of the effectiveness of the integrating action of the proposed FCS-MPC scheme and its comparison with the method described in [20].

A. Integral Terms Assessment

Two current-control tests at a constant speed ($\omega_m = 100\,\text{rpm}$) were performed to show the impact of including integral terms when a $+50\%$ error is introduced in both flux vector components ψ_d. In Figs. 9(a) and 9(b) the $d-$ and q-current reference tracking is shown when the integral term is considered (green lines) and not considered (blue lines). The numerical integration of the current errors (see (9)) is also computed and plotted in Figs. 9(c), and 9(d) to make the results clearer. Analyzing these figures, it is evident that including the integral term in the cost function allows for achieving zero steady-state current error, even in the presence of model inaccuracies. As a result, a high degree of robustness is achieved and potential parameter variations, model mismatches, etc., are successfully tackled by the controller.

To provide more insight, further tests were conducted to compare the effectiveness of the explicit integrating action

This article has been accepted for publication in IEEE Transactions on Industry Applications. This is the author's version which has not been fully edited and content may change prior to final publication. Citation information: DOI 10.1109/TIA.2022.3213002

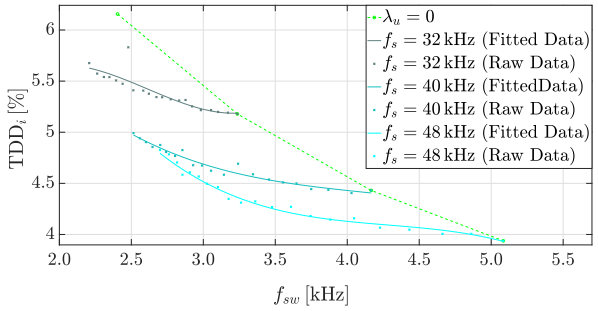

Fig. 11: Trade-off curve between current TDD_i and switching frequency ($i_d = i_q = 5.5\,\text{A}$; $\omega_m = 100\,\text{rpm}$, $0 < \lambda_u < 0.032$).

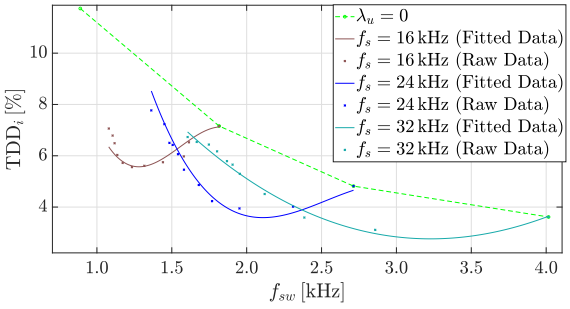

Fig. 13: Trade-off curve between current TDD_i and switching frequency at various λ_u ($i_d = i_q = 1.1\,\text{A}$; $\omega_m = 400\,\text{rpm}$, $0 < \lambda_u < 0.08$).

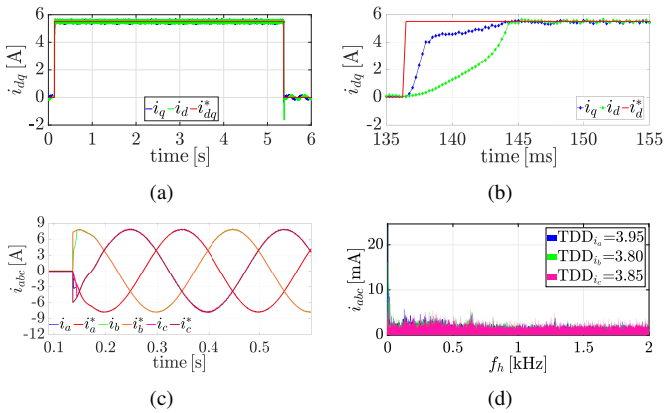

Fig. 12: (a) dq-current reference tracking ($f_s = 48\,\text{kHz}$, $\bar{f}_{sw} \approx 3.2\,\text{kHz}$, and $\lambda_u = 0.0160$). (b) dq-current reference tracking during transients. (c) a-, b-, and c-phase currents reference tracking. (d) a-, b-, and c-phase current harmonic spectra.

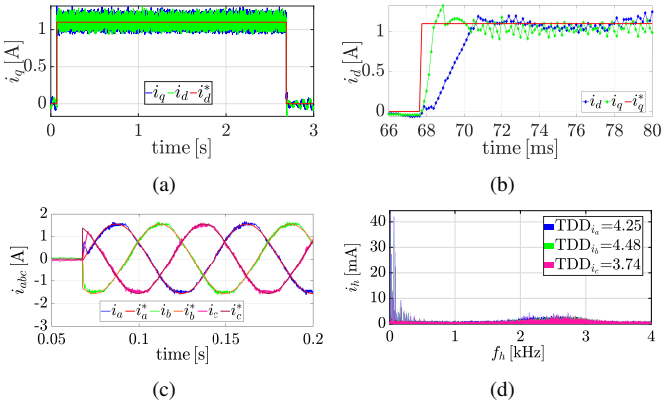

Fig. 14: (a) dq-current reference tracking ($f_s = 24\,\text{kHz}$, $\bar{f}_{sw} \approx 2\,\text{kHz}$, and $\lambda_u = 0.0160$). (b) dq-current reference tracking during transients. (c) a-, b-, and c-phase currents reference tracking. (d) a-, b-, and c-phase current harmonic spectra.

of the proposed FCS-MPC scheme with that of the method described in [20]. Even though both the proposed FCS-MPC scheme and the one in [20] include an element of integrating nature in the cost function, this is done differently. Specifically, the proposed method introduces the product between the predicted and accumulated errors—see (8) and (9), respectively—that can enable faster transient responses. To verify this, the tests were carried out by considering that the flux was overestimated by 30% while operating in the current-control mode and at a constant speed. The d-and q-current references were set to $i_d = 2.6\,\text{A}$, and $i_q = 3.7\,\text{A}$, respectively, corresponding to a torque command of $T_{em} = 7\,\text{Nm}$. Moreover, the rotational speed was $800\,\text{rpm}$, and the dc-link voltage $300\,\text{V}$. Finally, the sampling frequency was $24\,\text{kHz}$, and the control effort weighting factor was chosen as $\lambda_u = 0.0040$. For the first test, the integral of the current error was excluded from the cost function; the corresponding tracking of the q-component of the current reference is shown in Fig. 10. In the same figure, the tracking performance of the proposed FCS-MPC method is shown when the integrating term is active. Finally, for comparison purposes, the behavior of the method in [20] is depicted. As can be observed, both FCS-MPC methods successfully compensate for the error introduced in the prediction model due to the flux variation, but the proposed method exhibits better dynamic performance.

Finally, it is worth mentioning that the integral of the current error is calculated considering the predicted current error (see (8)) and the integral of the past errors (see (9)). As these depend on the (known) current reference and the (already computed) accumulated steady-state error, respectively, it can be seen that the additional computational overhead is very small, especially as compared with methods that rely on an augmented state or an exhaustive prediction of the state. Hence, the proposed method, not only selects the optimal actuating voltage vector by accounting for the past steady-state error (and thus by introducing an integrating element that improves the robustness), but it also comes with relatively low computational complexity.

B. Tests at Rated Current

The current references on the d-and q-axis were set equal to the rated value while the speed was fixed by the prime mover to $100\,\text{rpm}$. Fig. 11 reports the results in terms of TDD_i of the test campaign carried out at three different values of sampling frequency: $f_s = 32, 40$, and $48\,\text{kHz}$ over a wide range of switching frequencies. Similar to the simulation studies (see Fig. 6), the trend based on the experiments is the same, i.e., the

proposed FCS-MPC clearly outperforms the conventional one thanks to the fine granularity of switching. Fig. 12 reports the dq-current tracking, the phase currents, and harmonic spectra for the given operating point.

C. Tests at 20% of the Rated Current

In the second test campaign, the dq-axis current references were set to 20% of the rated current, while the rotational speed was set to 400 rpm. As for the previous set of tests, the trend illustrated in Fig. 13 shows that more favorable TDD$_i$s can be achieved with the proposed FCS-MPC algorithm. However, differently from the previous case, the trends for the three tested sampling frequencies $f_s = 16$, 24, and 32 kHz show a different behavior because they are not monotonically decreasing as the switching frequency increases. This difference can be justified by the non-linear inductance variations with the current which is an intrinsic characteristic of the SyRel machine. Finally, the dq-reference current tracking, the phase currents, and the harmonic spectra are shown in Fig. 14.

D. Tests over the Entire d-q Current Plane

In the following, an experimental investigation of the steady-state performance over the entire dq current plane is reported for two different values of the control effort weighting factor, i.e., $\lambda_u = 0$ and $\lambda_u = 0.0160$, when considering a fixed speed of 400 rpm and a sampling frequency of $f_s = 48$kHz. A comprehensive performance metric, c_k, is considered to compare these two series of tests, defined as the product of TDD$_i$ and $\bar{f}_{sw}$.

$$c_k = \text{TDD}_i \bar{f}_{sw}. \tag{12}$$

The performance metric c_k takes into account both the effect of the switching frequency and the TDD$_i$. Lower c_k values mean better overall performance.

In Fig. 15, the obtained c_k is plotted for the two cases $\lambda_u = 0$ and $\lambda_u = 0.016$. It can be noticed how the c_k variations are mainly due to the d-current component variation as the L_{dd} variation over the tested current domain is more significant than L_{qq} (see Fig. 3). In general, high performance is achievable in the whole current operating region by setting $\lambda_u > 0$.

E. Tests at Different Speeds

Speed variations also have an impact on the overall performance. For this reason, current control tests were performed to quantify the importance of this variation for two values of the control effort weighting factor ($\lambda_u = 0, \lambda_u = 0.0160$). In this case, the tests were performed with a fixed sampling frequency ($f_s = 48$ kHz) and both current references i_d and i_q to 1.1 A, while the rotational speeds varied from 100 rpm to 900 rpm with a 100 rpm speed step. The TDD$_i$ and $\bar{f}_{sw}$ trends over the rotational speed ω_m are represented in Fig. 16(a), showing more profitable results when $\lambda_u = 0.0160$. Fig. 16(b) shows the c_k trend for different speeds. Lower c_k is observable with $\lambda_u = 0.0160$ when $\omega_m > 750$ rpm. This is because the back-electromotive force term in (3) is more significant than the control effort in (7) to increase the granularity of switching.

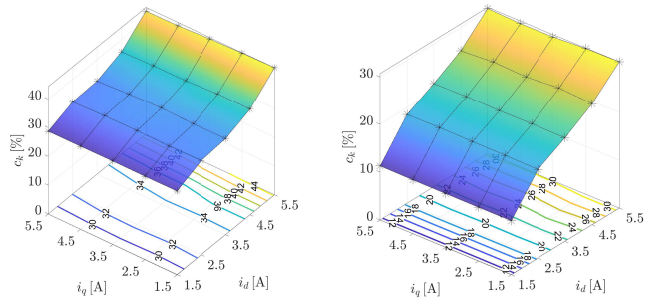

(a) (b)

Fig. 15: (a) Overall steady-state performance over the current domain at $\omega_m = 100$ rpm, $f_s = 48$ kHz, and $\lambda_u = 0$. (b) Overall steady-state performance over the current domain at $\omega_m = 100$ rpm, $f_s = 48$ kHz, and $\lambda_u = 0.016$.

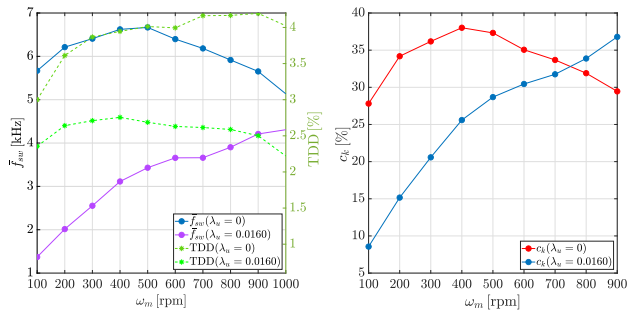

Fig. 16: (a) TDD$_i$ and $\bar{f}_{sw}$ trends with respect to the speed for a fixed $\lambda_u = 0$. (b) TDD$_i$ and $\bar{f}_{sw}$ trends with respect to the speed for a fixed $\lambda_u = 0.016$.

F. Tests at MTPA Conditions

Without changing the inner (FCS-MPC-based) control loop, the current references corresponding to a specific electromagnetic torque demand are selected according to the MTPA (see Fig. 4). Two torque control tests ($T_{em} = 1.4$Nm, and $T_{em} = 12.6$Nm) were performed and compared for various f_s and λ_u in Fig. 17.

Lower TDD$_i$ is achieved for lower torque when considering the same switching frequency. In addition, a lower margin of improvement can be achieved by varying λ_u when considering high torque values. Indeed, with higher torque, the current reference tracking term in (7) dominates the control effort, decreasing the margin of improvement.

VI. Conclusions

In this work, an improved finite control set model predictive controller (FCS-MPC) was implemented and tested on a SyRel motor drive. It was shown how the performance of a highly non-linear drive can be significantly improved by adopting a FCS-MPC with a cost function consisting of three terms: the typical reference tracking term, an integral term of the current tracking error that depends on the actuating commands, and a control effort term. The proposed integral term is able to compensate for any system non-idealities and unmodeled dynamics which could negatively affect the system performance, at the cost of only a small computational overhead. Lower

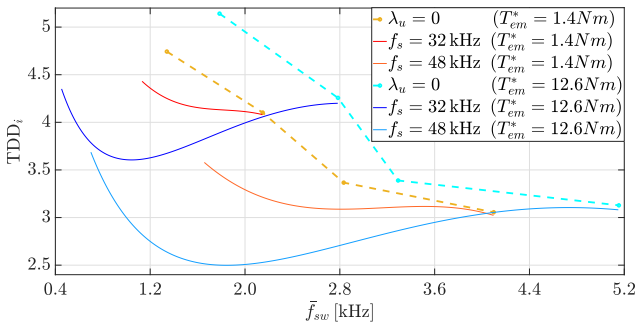

Fig. 17: TDD_i and switching frequency trade-off for two torque references ($\omega_m = 100\,\text{rpm}$, $0 < \lambda_u < 0.032$).

output current distortions and granularity of switching are achieved, enabling a favorable operation with reduced power losses thanks to the direct control of the switching frequency. Several design insights were provided by analyzing the steady-state performance under different values of the control effort weighting factor (i.e., at different switching frequencies) and sampling frequencies. An extensive test campaign endorses the proposed control approach and assesses its validity for a wide variety of operating conditions.

In a future step, the design and implementation aspects of the proposed control method can be further investigated. Among those, the tuning process of several weighting factors is a relevant research topic. Even though such terms are typically tuned by examining the Pareto optimal points [8], the multidimensional tradeoff curves do not allow for a straightforward design procedure. Moreover, to further increase the switching granularity, an FPGA-based implementation of the controller could be considered. Due to the nature of the solution process, i.e., exhaustive enumeration, many operations can be parallelized with such an implementation approach. In doing so, higher sampling frequencies—and, consequently, switching granularity—can be achieved as the control cycle can be further reduced.

REFERENCES

[1] A. Boglietti, A. Cavagnino, M. Pastorelli, D. Staton, and A. Vagati, "Thermal analysis of induction and synchronous reluctance motors," *IEEE Transactions on Industry Applications*, vol. 42, no. 3, pp. 675–680, 2006.

[2] A. Vagati, M. Pastorelli, G. Franceschini, and C. Petrache, "Design of low-torque-ripple synchronous reluctance motors," in *IAS '97. Conference Record of the 1997 IEEE Industry Applications Conference Thirty-Second IAS Annual Meeting*, vol. 1, pp. 286–293 vol.1, 1997.

[3] I. Nasui-Zah, A.-M. Nicorici, and C. Marţis, "Saturation and cross-saturation in synchronous reluctance machines," in *2018 International Conference and Exposition on Electrical And Power Engineering (EPE)*, pp. 0347–0351, 2018.

[4] N. Bianchi, S. Bolognani, E. Carraro, M. Castiello, and E. Fornasiero, "Electric vehicle traction based on synchronous reluctance motors," *IEEE Transactions on Industry Applications*, vol. 52, no. 6, pp. 4762–4769, 2016.

[5] S. Ferdous, P. Garcia, M. A. M. Oninda, and M. A. Hoque, "MTPA and field weakening control of synchronous reluctance motor," in *2016 9th International Conference on Electrical and Computer Engineering (ICECE)*, pp. 598–601, 2016.

[6] G. H. B. Foo and X. Zhang, "Robust direct torque control of synchronous reluctance motor drives in the field-weakening region," *IEEE Transactions on Power Electronics*, vol. 32, no. 2, pp. 1289–1298, 2017.

[7] P. Karamanakos, E. Liegmann, T. Geyer, and R. Kennel, "Model predictive control of power electronic systems: Methods, results, and challenges," *IEEE Open Journal of Industry Applications*, vol. 1, pp. 95–114, 2020.

[8] P. Karamanakos and T. Geyer, "Guidelines for the design of finite control set model predictive controllers," *IEEE Transactions on Power Electronics*, vol. 35, no. 7, pp. 7434–7450, 2020.

[9] J. Riccio, P. Karamanakos, S. Odhano, M. Tang, M. D. Nardo, and P. Zanchetta, "A direct model predictive control strategy for high-performance synchronous reluctance motor drives," in *2021 IEEE Energy Conversion Congress and Exposition (ECCE)*, pp. 4704–4710, 2021.

[10] C. Scognamillo, A. P. Catalano, A. Borghese, M. Riccio, V. d'Alessandro, G. Breglio, A. Irace, R. N. Tripathi, A. Castellazzi, and L. Codecasa, "Electrothermal modeling, simulation, and electromagnetic characterization of a 3.3 kV SiC mosfet power module," in *2021 33rd International Symposium on Power Semiconductor Devices and ICs (ISPSD)*, pp. 123–126, 2021.

[11] A. Borghese, A. P. Catalano, M. Riccio, L. Codecasa, A. Fayyaz, V. d'Alessandro, A. Castellazzi, L. Maresca, G. Breglio, and A. Irace, "An efficient simulation methodology to quantify the impact of parameter fluctuations on the electrothermal behavior of multichip SiC power modules," in *Silicon Carbide and Related Materials 2018*, ser. Materials Science Forum, vol. 963, pp. 855–858. Trans Tech Publications Ltd, 9 2019.

[12] C.-K. Lin, J.-t. Yu, Y.-S. Lai, and H.-C. Yu, "Improved model-free predictive current control for synchronous reluctance motor drives," *IEEE Transactions on Industrial Electronics*, vol. 63, no. 6, pp. 3942–3953, 2016.

[13] R. Vargas, U. Ammann, and J. RodrÍguez, "Predictive approach to increase efficiency and reduce switching losses on matrix converters," *IEEE Transactions on Power Electronics*, vol. 24, no. 4, pp. 894–902, 2009.

[14] L. Ortombina, E. Liegmann, P. Karamanakos, F. Tinazzi, M. Zigliotto, and R. Kennel, "Constrained long-horizon direct model predictive control for synchronous reluctance motor drives," in *2018 IEEE 19th Workshop on Control and Modeling for Power Electronics (COMPEL)*, pp. 1–8, 2018.

[15] G. Cimini, D. Bernardini, A. Bemporad, and S. Levijoki, "Online model predictive torque control for permanent magnet synchronous motors," in *2015 IEEE International Conference on Industrial Technology (ICIT)*, pp. 2308–2313, 2015.

[16] J. Rodriguez, M. P. Kazmierkowski, J. R. Espinoza, P. Zanchetta, H. Abu-Rub, H. A. Young, and C. A. Rojas, "State of the art of finite control set model predictive control in power electronics," *IEEE Transactions on Industrial Informatics*, vol. 9, no. 2, pp. 1003–1016, 2013.

[17] A. Favato, P. G. Carlet, F. Toso, and S. Bolognani, "A model predictive control for synchronous motor drive with integral action," in *IECON 2018 - 44th Annual Conference of the IEEE Industrial Electronics Society*, pp. 325–330, 2018.

[18] L. Ortombina, P. Karamanakos, and M. Zigliotto, "Robustness analysis of long-horizon direct model predictive control: Induction motor drives," in *2020 IEEE 21st Workshop on Control and Modeling for Power Electronics (COMPEL)*, pp. 1–8, 2020.

[19] S. Hanke, S. Peitz, O. Wallscheid, J. Böcker, and M. Dellnitz, "Finite-control-set model predictive control for a permanent magnet synchronous motor application with online least squares system identification," in *2019 IEEE International Symposium on Predictive Control of Electrical Drives and Power Electronics (PRECEDE)*, pp. 1–6, 2019.

[20] R. P. Aguilera, P. Lezana, and D. E. Quevedo, "Finite-control-set model predictive control with improved steady-state performance," *IEEE Transactions on Industrial Informatics*, vol. 9, no. 2, pp. 658–667, 2013.

[21] E. Armando, R. I. Bojoi, P. Guglielmi, G. Pellegrino, and M. Pastorelli, "Experimental identification of the magnetic model of synchronous machines," *IEEE Transactions on Industry Applications*, vol. 49, no. 5, pp. 2116–2125, 2013.

[22] H. Hadla and S. Cruz, "Predictive stator flux and load angle control of synchronous reluctance motor drives operating in a wide speed range," *IEEE Transactions on Industrial Electronics*, vol. 64, no. 9, pp. 6950–6959, 2017.

[23] Y. Zhao, L. Ren, Z. Liao, and G. Lin, "A novel model predictive direct torque control method for improving steady-state performance of the synchronous reluctance motor," *Energies*, vol. 14, no. 8, 2021.
[24] B. Stellato, T. Geyer, and P. J. Goulart, "High-speed finite control set model predictive control for power electronics," *IEEE Transactions on Power Electronics*, vol. 32, no. 5, pp. 4007–4020, 2017.
[25] A. Galassini, G. Lo Calzo, A. Formentini, C. Gerada, P. Zanchetta, and A. Costabeber, "uCube: Control platform for power electronics," in *2017 IEEE Workshop on Electrical Machines Design, Control and Diagnosis (WEMDCD)*, pp. 216–221, 2017.

Jacopo Riccio received his B.Sc. and M.Sc. degrees in mechanical engineering from the University of "Roma Tre", Italy, in 2014 and 2018, respectively. From 2017 to 2018, he joined the Department of Electrical and Electronics Engineering, at the University of Nottingham as a research associate. Since December 2018, he is with the Power Electronics and Machine Control Group of the University of Nottingham as a Ph.D. student. His research interests include the control of electric drives based on model-based predictive control and sensorless algorithms.

Petros Karamanakos (S'10 – M'14 – SM'19) received the Diploma and Ph.D. degrees in electrical and computer engineering from the National Technical University of Athens (NTUA), Athens, Greece, in 2007, and 2013, respectively.

From 2010 to 2011 he was with the ABB Corporate Research Center, Baden-Dättwil, Switzerland, where he worked on model predictive control strategies for medium-voltage drives. From 2013 to 2016 he was a PostDoc Research Associate in the Chair of Electrical Drive Systems and Power Electronics, Technische Universität München, Munich, Germany. Since 2016, he has been with the Faculty of Information Technology and Communication Sciences, Tampere University, Tampere, Finland, where he is currently an Associate Professor. His main research interests lie at the intersection of optimal control, mathematical programming and power electronics, including model predictive control and optimal modulation for power electronic converters and ac variable speed drives.

Dr. Karamanakos received the 2014 Third Best Paper Award of the IEEE Transactions on Industry Applications and two Prize Paper Awards at conferences. He serves as an Associate Editor of the IEEE Transactions on Industry Applications and of the IEEE Open Journal of Industry Applications. He is a Regional Distinguished Lecturer of the IEEE Power Electronics Society in the years 2022 and 2023.

Mauro Di Nardo (M'18) received the M.Sc. (Hons.) degree in electrical engineering from the Polytechnic University of Bari, Italy, in 2012, and the Ph.D. degree in electrical machine design from the University of Nottingham, U.K., in 2017. From 2017 to 2019, he was Head with the AROL R&D Team within the Polytechnic University of Bari leading industrial projects on electrical drives design for mechatronics applications. Since the 2019, he is with the Power Electronics and Machine Control Group of the University of Nottingham as Research Fellow working on wide variety of projects. His research interests include the analysis, modelling, design optimizations and experimental characterization of permanent magnet and synchronous reluctance machines for automotive, aerospace and household sectors, induction motor for industrial applications as well as niche machine topologies such as bearingless and hysteresis motor. He serves as an Associate Editor for the Open Journal of Industry Applications.

Shafiq Odhano (S'13–M'15–SM'20) received the M.Sc. degree in electrical engineering and the Ph.D. degree in power electronics, machines, and drives from the Politecnico di Torino, Turin, Italy, in 2014. He has been affiliated with the Politecnico di Torino as a postdoctoral research fellow and with the University of Nottingham, UK, as a research fellow. He is currently a lecturer in electric drives at Newcastle University, Newcastle Upon Tyne, UK. His research interests include high-performance control of servo-drives, model predictive control of power converters, and self-commissioning of ac motor drives.

Mi Tang (M'16) received the M.Sc. degree in electrical engineering and Ph.D. degree in electrical and electronic engineering from the University of Nottingham, Nottingham, U.K., in 2012 and 2017, respectively. She is currently a Research Fellow with the Power Electronics, Machine and Control Group, University of Nottingham, Nottingham, U.K. Her research interests include deadbeat control, fault-tolerant control and repetitive control. She serves as an associate editor for IEEE transactions on industry applications from 2022.

Pericle Zanchetta (M '00, SM '15, F '19) received his MEng degree in Electronic Engineering and his Ph.D. in Electrical Engineering from the Technical University of Bari (Italy) in 1993 and 1997 respectively. In 1998 he became Assistant Professor of Power Electronics at the same University. In 2001 he became lecturer in control of power electronics systems in the PEMC research group at the University of Nottingham – UK, where he is now Professor in Control of Power Electronics systems. He is also part time professor at the University of Pavia, Italy. He has published over 350 peer reviewed papers, he has been Chair of the IEEE-IAS Industrial Power Converter Committee IPCC (2016-2017), Transactions review chair for IPCC (2018-2021). He was also Chair of the IEEE-IAS Industrial Power Conversion Systems Department IPCSD (2020-2021) and editor in chief of the IEEE Open Journal of Industry Applications. His research interests include control and optimization of power converters and drives, Matrix and multilevel converters. He is IEEE Fellow class 2019.